Free Energy and Temperature Dependence of Electron Transfer at the Metal-Electrolyte Interface

CHRISTOPHER E. D. CHIDSEY

The rate constant of the electron-transfer reaction between a gold electrode and an electroactive ferrocene group has been measured at a structurally well-defined metal-electrolyte interface at temperatures from 1° to 47°C and reaction free energies from −1.0 to +0.8 electron volts (eV). The ferrocene group was positioned a fixed distance from the gold surface by the self-assembly of a mixed thiol monolayer of $(\eta^5C_5H_5)Fe(\eta^5C_5H_4)CO_2(CH_2)_{16}SH$ and $CH_3(CH_2)_{15}SH$. Rate constants from 1 per second (s^{-1}) to 2×10^4 s^{-1} in 1 molar $HClO_4$ are reasonably fit with a reorganization energy of 0.85 eV and a prefactor for electron tunneling of 7×10^4 s^{-1} eV^{-1}. Such self-assembled monolayers can be used to systematically probe the dependence of electron-transfer rates on distance, medium, and spacer structure, and to provide an empirical basis for the construction of interfacial devices such as sensors and transducers that utilize macroscopically directional electron-transfer reactions.

LONG-DISTANCE, INTERFACIAL ELECTRON transfer plays a central role in such diverse processes as the bioenergetics of photosynthesis and respiration, the dye-sensitization of photographic materials, the collection of minority carriers at semiconductor photoelectrodes, and the direct amperometric detection of analytes with enzyme-modified electrodes. However, few well-defined experimental systems have been available to probe such fundamental issues as the dependence of interfacial electron-transfer rates on the reaction free energy, the electron-transfer distance, or the molecular structure of the interface. Li and Weaver have shown that the rate of electron transfer between an electrode and an electroactive group tethered to the surface through a carbon chain drops off exponentially with the chain length (*1*). Further study of that system was handicapped by the unknown and possibly heterogeneous structure of the interface. In contrast, rigid, structurally well-defined molecules containing two or more electroactive sites have been used to study intramolecular electron transfer for several years now (*2*).

Here, I report measurements of the interfacial electron-transfer rate between a gold electrode and an electroactive ferrocene group held a fixed separation from the electrode by a monolayer (Fig. 1). This previously characterized interface (*3*) is prepared by the self-assembly of alkane thiol derivatives on Au (*4–7*) and has been inferred (*3*) to have the same structure as the unsubstituted alkane thiol monolayers on Au(111) (*8–11*). In this report, the ferrocene sites are shown to be kinetically homogeneous, and the forward and backward electron-transfer rates (k_f and k_b, respectively) are measured over a large range of potentials, allowing the thermal activation and electron tunneling components of this prototypical interfacial electron-transfer reaction to be separately determined.

The samples are prepared by incubating freshly vapor-deposited Au mirrors for 2 days in a coadsorption solution of a ferrocene-terminated alkane thiol [0.1 mM $(\eta^5C_5H_5)Fe(\eta^5C_5H_4)CO_2(CH_2)_{16}SH$] and an unsubstituted alkane thiol [0.9 mM $CH_3(CH_2)_{15}SH$] in ethanol, followed by at least 10 days in an "exchange solution" of 1 mM $CH_3(CH_2)_{15}SH$ in ethanol to replace loosely bound ferrocene-terminated alkane thiols with unsubstituted thiols (*3*). Finally, the samples are placed in an electrochemical cell with 1 M aqueous $HClO_4$, a Ag/(1 mM $AgClO_4$, 1 M $HClO_4$) reference electrode, and a Pt counterelectrode (*3*).

The reduction and subsequent reoxidation of an electroactive group at a metal electrode is written (*12*)

$$\mathrm{ox} + e^- \underset{k_b}{\overset{k_f}{\rightleftarrows}} \mathrm{red} \qquad (1)$$

where ox is the oxidized form of the electroactive group (the cationic ferricenium group in this work) and red is the reduced form (the ferrocene group). The reaction free energy ΔG^0 is:

$$\Delta G^0 = e(E - E^{0'}) \qquad (2)$$

where e is the electron charge, E is the electrode potential, and $E^{0'}$ is the formal potential of the electroactive group. When $E = E^{0'}$, $k_f = k_b$. In general, k_f is expected to increase rapidly with decreasing reaction free energy, and k_b is expected to increase rapidly with increasing reaction free energy. Both the energetics and kinetics of the reaction can thus be conveniently varied by changing E (*13*).

In Fig. 2, the electrode potential is first scanned positively through $E^{0'}$ to oxidize the ferrocene to ferricenium (positive current peaks) and then scanned negatively to reduce the ferricenium back to ferrocene (negative current peaks). At the slowest scan

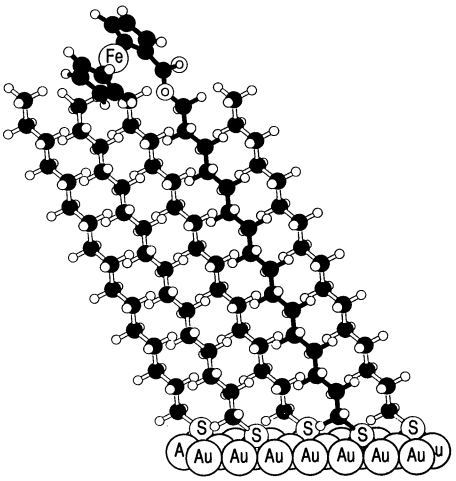

Fig. 1. Inferred structure of the monolayer formed by coadsorption of a ferrocene-terminated alkane thiol (highlighted with black bonds) and an unsubstituted alkane thiol on Au(111). The conformation about the ester group is chosen to illustrate the closest approach of the ferrocene group to the electrode, ~20 Å.

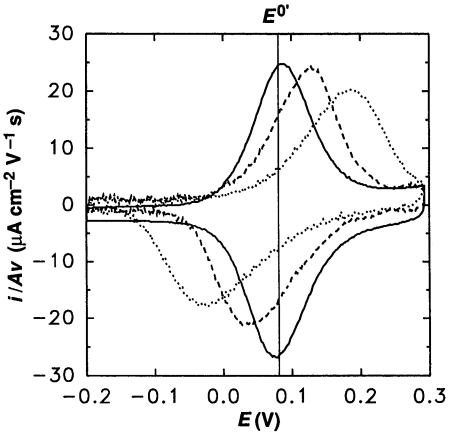

Fig. 2. Cyclic voltammograms of a mixed monolayer of ferrocene-terminated alkane thiol and unsubstituted alkane thiol on gold. The current i is normalized by the electrode area, A = 0.70 cm^2, and potential scan with rate v: 10 mV s^{-1} (solid), 120 mV s^{-1} (dashed), and 500 mV s^{-1} (dotted). The formal potential of the ferrocene group, $E^{0'}$, is indicated by the vertical line. Potentials are measured relative to a Ag/(1 mM $AgClO_4$, 1 M $HClO_4$) reference electrode.

AT&T Bell Laboratories, Murray Hill, NJ 07974.

rate (10 mV s^{-1}), the positive and negative current peaks occur at almost the same potential, indicating that the monolayer remains nearly at equilibrium with the electrode throughout the experiment. The full-widths at half-maximum of the peaks are ~95 mV, very close to the ideal (entropically determined) value of 90 mV expected for identical, independent sites at room temperature (*12*). At higher scan rates, the positive and negative current peaks split apart substantially, indicating that the scan rate is now comparable to the rates of electron transfer (*14*). These peak splittings can be converted to a standard electron-transfer rate constant, $k^0 = 1.3\ s^{-1}$, by the formalism of Laviron (*3, 15*) However, the formalism assumes a particular potential dependence of the rate. The current transient following a potential step is a more direct measure of the kinetics.

If the current transients are slow enough to be accurately recorded, the potential-step experiment has three important advantages: (i) the kinetics for different potentials (that is, different reaction free energies) are not convoluted by a potential scan; (ii) the kinetic homogeneity of the sites can be judged by the functional form of the current transient (for the reaction in Eq. 1, the decay of the electron-transfer current should be a single exponential with a decay rate constant of $k_f + k_b$); and (iii) the rates can be measured far from $E^{0'}$ (that is, at large positive or negative reaction free energy).

An example of the potential-step experiment is shown in Fig. 3A. After a step from $E^{0'}$ to a more negative potential, there is initially a short current transient due to charging the electrochemical double layer, and then the electron-transfer current decays on the time scale of seconds. Following a step back to $E^{0'}$, a current transient of opposite sign is observed. Semi-logarithmic plots of current transients at different final potentials are shown in Fig. 3, B to D. With the exception of the initial double-layer charging currents, the semilog plots are linear to the noise level, indicating that the electron-transfer current decays as a single exponential. The data in Fig. 3B, obtained with a low-pass filter to provide greater dynamic range, are fit by one exponential over three orders of magnitude, a good indication of the kinetic homogeneity of the ferrocene sites.

A semi-log plot of measured decay rate constants as a function of the applied electrode potential at 25°C is shown in Fig. 4A. The rate constants were determined by linear regression of unfiltered electron-transfer current transients such as those in Fig. 3, C and D. The experimental potential limits are imposed by several factors, including the decay rate of the signal, interfering electrochemical reactions, and the onset of sample degradation. Measured decay rate constants at three temperatures, 1°, 25°, and 47°C, are shown in Fig. 4B. Near $E^{0'}$, the rate constant changes by a factor of 3.7 between 1° and 47°C. At more positive or negative potentials, the rate is less strongly dependent on temperature.

The lines plotted in Fig. 4 are calculated rate constants for different models of the electron-transfer kinetics. The dotted curve in Fig. 4A is a plot of the decay rate constant predicted by the Butler-Volmer relation (*12*), a time-honored parameterization of the potential dependence of electrochemical rates.

$$k_f + k_b = k^0 \exp[+\alpha e(E - E^{0'})/(k_B T)] + k^0 \exp[-(1 - \alpha)e(E - E^{0'})/(k_B T)] \quad (3)$$

where k^0 is the standard rate constant, α is the transfer coefficient, k_B is the Boltzmann constant, and T is the absolute temperature. The symmetry of the data, the minimum at $E^{0'}$, and the slope near $E^{0'}$ are reproduced by the curve. However, the Butler-Volmer parameterization cannot account for the curvature far from $E^{0'}$ and does not incorporate the temperature dependence of k^0 explicitly. For these attributes, we turn to the contemporary theory of electron transfer.

An extensive theory of one-electron, outer-sphere electron-transfer reactions at electrodes and between molecules has been developed over the last four decades (*16–21*). Three aspects of the specific reaction considered here are of particular importance: (i) because one of the partners in the reaction is a metal with a continuum of electronic states, k_f and k_b will be sums of the individual rates for each electronic state of the metal weighted by the Fermi-Dirac probability of occupancy (f_+) or vacancy (f_-) of that state;

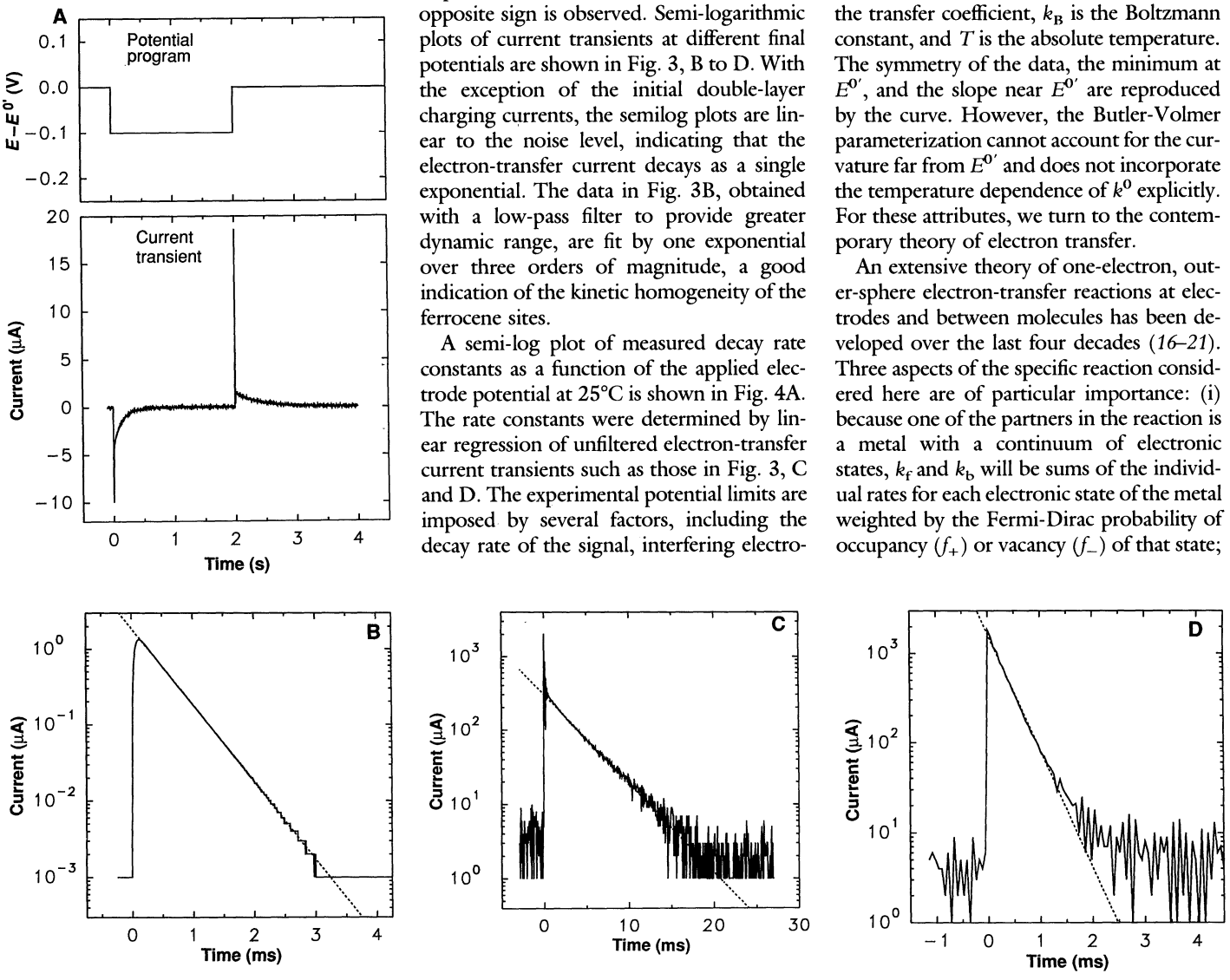

Fig. 3. (**A**) Example of potential-step experiment showing current transients composed of a rapidly decaying double-layer charging current and a slower electron-transfer current. (**B** to **D**) Semi-logarithmic plots of the absolute value of the current following potential steps to various potentials (solid) and linear regression fits to the linear portions (dashed). Potential versus $E^{0'}$, decay rate constant: (B) 0.0 V, 2.33 s^{-1} (filtered with a 30-ms time constant); (C) +0.323 V, 276 s^{-1}; and (D) −0.577 V, 2980 s^{-1}.

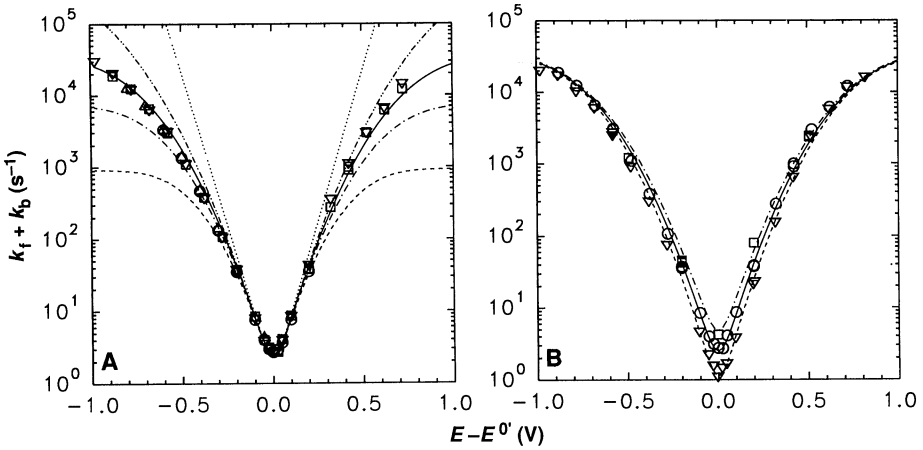

Fig. 4. (**A**) Semi-log plot of the measured decay rate constants at 25°C for four samples (symbols) and calculated decay constants from Eq. 3 with $k^0 = 1.25\ s^{-1}$, $\alpha = 0.5$ (dotted); and from Eq. 7 and 8 with: $\lambda = 1.1$ eV, $\upsilon\rho = 7.48 \times 10^5\ s^{-1}\ eV^{-1}$ (dot-dot-dashed); $\lambda = 0.85$ eV, $\upsilon\rho = 6.73 \times 10^4\ s^{-1}\ eV^{-1}$ (solid); $\lambda = 0.7$ eV, $\upsilon\rho = 1.55 \times 10^4\ s^{-1}\ eV^{-1}$ (dot-dashed); and $\lambda = 0.5$ eV, $\upsilon\rho = 2.29 \times 10^3\ s^{-1}\ eV^{-1}$ (dashed). (**B**) Semi-log plot of the measured decay rate constants at: 1°C (triangles), 25°C (circles), and 47°C (squares); and calculated decay constants from Eq. 7 and 8 with $\lambda = 0.85$ eV, $\upsilon\rho = 6.73 \times 10^4\ s^{-1}\ eV^{-1}$.

(ii) because the electron must tunnel a long distance, the transition rate in the activated complex is expected to be determined by the electronic coupling between the metallic states of the electrode and the ferrocene group (that is, the reaction should be nonadiabatic); and (iii) because ferrocene and the ferricenium cation have similar structures, the domiant contribution to the activation barrier is expected to be the reorganization of the solvent (*22*), which can be treated classically.

The rate constants k_f and k_b can thus be written

$$k_{f,b} = \sum_i f_{\pm}(\varepsilon_i)\,\upsilon_i \exp[-\Delta G^{\ddagger}_{f,b}(\varepsilon_i)/(k_B T)] \quad (4)$$

where $-e\varepsilon_i$ is the energy of the ith metallic state. The Fermi-Dirac probabilities are

$$f_{\pm}(\varepsilon_i) = \{1 + \exp[\pm e(E - \varepsilon_i)/(k_B T)]\}^{-1} \quad (5)$$

The prefactor υ_i is determined by the electronic coupling between the ith metallic state and the ferrocene group. The activation free energies are given by the Marcus relation (*19*)

$$\Delta G^{\ddagger}_{f,b}(\varepsilon_i) = [\lambda \pm e(\varepsilon_i - E^{0'})]^2/(4\lambda) \quad (6)$$

where λ is the reorganization energy, the free energy needed to distort the atomic positions of the reactant and its solvation shell to the atomic positions of the product and its solvation shell without allowing the electron to transfer. It is assumed that the same reorganization energy applies to both the forward and backward reactions (see below).

Making the simplifying assumption that both the electronic coupling and the density of metallic states are independent of energy (see below), Eq. 4 can be recast as

$$k_{f,b} = \upsilon\rho(4\pi\lambda k_B T)^{1/2}\,\Omega_{f,b}(\lambda, E - E^{0'}, T) \quad (7)$$

where $(\upsilon\rho)ed\varepsilon$ is the prefactor for electron transfer between a ferrocene group and all metallic states in the energy interval $ed\varepsilon$, and $\Omega_{f,b}(\lambda, E - E^{0'}, T)$ are activation factors, which are independent of the electronic coupling, given by

$$\Omega_{f,b}(\lambda, E - E^{0'}, T) = C^{1/2}\int_{-\infty}^{\infty} g(x)dx \quad (8)$$

where $C = (k_b T/4\pi\lambda)$ and $g(x) =$

$$\frac{\exp\left\{-\left[x - \dfrac{\lambda \pm e(E - E^{0'})}{k_B T}\right]^2\left[\dfrac{1}{C\pi}\right]\right\}}{1 + \exp(x)}$$

At moderate reaction free energies and temperatures [$e(E - E^{0'}) << \lambda$, $k_B T << \lambda$], Ω_f and Ω_b are both much less than unity, normally activated, and follow opposing exponential dependencies on potential. At very negative reaction free energy, the forward activation factor, Ω_f, is unity and temperature independent; similarly, at very positive reaction free energy, Ω_b is unity and temperature independent.

The various dashed and solid curves in Fig. 4A are plots of $k_f + k_b$ from Eqs. 7 and 8 for several values of the reorganization energy λ. In all cases the product $\upsilon\rho$ is adjusted to give the measured decay rate constant of 2.5 s^{-1} at $E^{0'}$. The curve with $\lambda = 0.85$ eV and $\upsilon\rho = 6.73 \times 10^4\ s^{-1}\ eV^{-1}$ approximates the observed values quite well. The plateau behavior at high driving force is due to the continuum of states in the metal, and is in contrast to the case of electron transfer between two molecular sites, where, at high driving force, the rate decreases as the reaction free energy is made more negative [the Marcus-inverted region (*2*)]. Curves obtained from the classical Marcus theory neglecting the continuum of metallic states do not fit the data at very positive and very negative potentials. The parameters that give the best fit in Fig. 4A are used to generate the curves for 1°, 25°, and 47°C plotted in Fig. 4B. These curves reproduce well the experimental temperature dependence at $E^{0'}$ and the decrease of that dependence at both more positive and more negative potentials.

From the agreement of the data and the theoretical curves in Fig. 4B, Eqs. 7 and 8 are apparently adequate to describe this interfacial electron-transfer reaction. In particular, two of the assumptions made now appear to be reasonable: (i) the reorganization energy for the forward and backward reactions are apparently quite similar, or the data would not be as symmetric as they are; and (ii) the product of the tunneling rate in the activated complex and the density of states is apparently approximately independent of the energy of the metallic state, or the limiting rate constants would be different for the positive and negative branches in Fig. 4B.

From the value obtained for $\upsilon\rho$, one can estimate a coupling of about 10^{-6} eV between the metallic states and the ferrocene group (*23, 24*), a small value that justifies treating the reaction as nonadiabatic. The distance dependence of this coupling will be described elsewhere (*25*). The reorganization energy of 0.85 eV determined here compares reasonably with the calculated solvent reorganization energy of 0.94 eV (*26*), indicating that, as expected, solvation is the dominant contributor to the activation.

Self-assembly of monolayers provides a dramatic improvement in the type of structures available at interfaces, offering the opportunity to control the kinetics of interfacial electron transfer. Self-assembled structures should allow novel interfacial chemistry to be explored. For instance, electroactive groups positioned so that they cannot be highly solvated could mimic, at a macroscopic interface, the weakly activated and directional electron-transfer reactions that are the key to efficient charge separation in natural photosynthetic membranes.

REFERENCES AND NOTES

1. T. T.-T. Li and M. J. Weaver, *J. Am. Chem. Soc.* **106**, 6107 (1984).